RESEARCH ON THE STAGGERED BATTERY THERMAL MANAGEMENT SYSTEM BASED ON AIR DISTRIBUTION PIPES

Jiayue CHEN [1,2],Guofu LI [1,2*]

[*1]School of Mechanical Engineering and Mechanics, Ningbo University, Ningbo, People's Republic of China

[2] Institute of Advanced Energy Storage Technology and Equipment, Ningbo University, Ningbo ,People' s Republic of China

[*] Guofu LI; E-mail: liguofu@nbu.edu.cn

Addressing the issues of temperature rise and inconsistent temperature uniformity in traditional staggered air-cooled battery thermal management systems, a novel cooling strategy based on air distribution pipes is proposed. By utilizing these pipes, cooling air is better distributed throughout the battery module, thereby compensating for the shortcomings of traditional structures in terms of cooling air distribution. Meanwhile, by taking advantage of the staggered arrangement, the problems of additional volume and complex piping that are commonly caused by the use of air distribution pipes are avoided, thus effectively making up for the shortcomings of the two methods. The results demonstrate that this design offers significant advantages over traditional structures. Based on this foundation, an optimization analysis has been conducted on the structural parameters of the air distribution device and those of the battery module. The findings reveal that when the module's air outlet is positioned directly above, with an outlet radius of 6.5 mm, a battery spacing of 2 mm, an air distribution pipe outlet size of 5×10 mm^2, and an angle between adjacent outlets of the air pipe of 40°, the BTMS exhibits optimal temperature performance. Specifically, Under the optimal configuration of structural parameters, when the charge/discharge rate reaches 2C, the maximum temperature of the battery module is 37.81°C the maximum temperature is reduced by 2.47 °C compared to the traditional structure, while the temperature difference is decreased by 74.5%.

Key words: air cooling system, staggered arrangement, air distribution pipe, structure optimization

1. Introduction

With technological advancements, batteries, as a more environmentally friendly energy storage component, have seen significant development and large-scale application in the fields of new energy vehicles and energy storage [1]. Lithium-ion batteries have emerged as the most popular choice among energy storage batteries due to their advantages such as high energy density, low self-discharge rate, long cycle life, and absence of memory effect [2, 3]. However, it is important to note that lithium-ion batteries are susceptible to temperature [4, 5]. In high-temperature environments, the internal resistance of lithium-ion batteries deteriorates significantly after charge-discharge cycles, and the battery degrades further as the cycle rate increases [6]. Additionally, high temperatures can lead to lithium inventory loss, anode material loss, and electrode interface degradation, all of which contribute to more severe cyclic degradation of the battery [7]. Meanwhile, when discharging in a low-temperature environment, the output power and capacity of the battery will correspondingly decrease due to the continuous increase in its internal impedance [8]. Therefore, when using lithium-ion batteries as a power source, it is crucial to equip a suitable battery thermal management system (BTMS).

During charging and discharging, batteries generate a significant amount of heat, which accumulates in the confined space over time. This heat can trigger subsequent abuse reactions [9], leading to further overheating of the battery and, under extreme conditions, even fires or explosions. Therefore, the goal of the BTMS is to utilize the limited space effectively, controlling the battery's temperature within a reasonable range through media such as air and coolant, while minimizing the temperature difference between batteries. Generally, the optimal operating temperature range for lithium-ion batteries is between 25°C and 40°C, with a temperature difference of no more than 5°C being ideal [10, 11].In the battery thermal management systems currently in use, there are two mainstream heat dissipation methods: air cooling [12, 13] and liquid cooling [14]. With the continuous development of research, subsequent methods such as PCM cooling [15], heat pipe cooling[16], and combinations of these have emerged. Air cooling has been widely adopted due to its advantages of low cost, no risk of coolant leakage, and minimal risk.

In the field of forced air cooling, research has largely focused on the geometry of air channels, battery arrangements, and airflow paths. Yang *et al.* [17] discussed the thermal performance of battery packs when cylindrical batteries were arranged in a staggered or aligned. By varying the longitudinal and lateral spacing between batteries, they found that increasing the longitudinal spacing reduced the average battery temperature, while increasing the lateral spacing improved temperature uniformity but led to higher temperature rise. Wang *et al.* [18] examined the thermal performance of battery modules with different cell layouts and fan positions. They discovered that the best heat dissipation performance was achieved when the fan was positioned at the top of the module and the rectangular cell layout was arranged in a 5×5 configuration. When considering space utilization, the hexagonal structure with 19 cells was the optimal choice. Lu *et al.* [19] proposed novel cooling channels and air supply strategies based on staggered battery pack arrangements. Through comprehensive analysis of maximum temperature, space utilization, and energy consumption, they determined that the optimal cooling channel size was 1 mm. The study also found that the air supply method was crucial in influencing the battery temperature distribution. Yang *et al.* [20] first analyzed various parameters of traditional staggered arrangements and then introduced reciprocating airflow for heat dissipation in battery modules based on this structure. Experimental results showed that reciprocating airflow was effective in reducing the maximum temperature and temperature difference within the battery module.

However, research on forced air cooling with air distribution pipes is relatively scarce, possibly due to the added complexity and cost these pipes introduce to battery thermal management systems. Zhou *et al.* [21] adopted a cooling structure that differed from traditional air cooling, utilizing air distribution pipes to meet the heat dissipation requirements of batteries during 3C and 4C charge/discharge rates. They found that increasing the diameter and number of rows of perforated plates in the design helped reduce the maximum temperature and improve temperature uniformity without increasing power consumption. Yang *et al.* [22] designed a honeycomb-like heat dissipation structure equipped with air distribution plates and bionic heat sinks, identifying the optimal distribution channels to enhance battery temperature uniformity. While these air distribution structures effectively addressed the issue of cooling airflow distribution, they were relatively complex and may have increased the battery pack's volume, thereby reducing space utilization.

Inspired by their work, this paper introduces air distribution pipes into the staggered arrangement structure, aiming to resolve issues such as elevated temperature and large temperature differences inherent in traditional staggered structures through the cooperation between the pipes and the module structure. Leveraging the characteristics of the staggered structure, the air distribution pipes are placed in the extra spaces within the staggered arrangement. Since the original battery arrangement remains unchanged, the space utilization of the battery module does not decrease. Furthermore, as the air distribution pipes do not directly contact the batteries, the reliability of the thermal management system is ensured. Based on this concept, a CFD three-dimensional battery model has been established and validated through experiments. This model is then utilized to investigate the impact of the battery module structure and air distribution pipe configuration on the thermal management system. This paper provides designers with a novel approach to battery thermal management systems featuring air distribution pipes.

2. Battery module and simulation

2.1. Battery Pack and Air Distribution Pipe Structure

As shown in fig. 1(a), the battery pack with air distribution pipes comprises 35 individual cells. The cooling air flows into the air distribution pipes from the upper inlet, then flows through the pipes to various parts of the battery pack for heat dissipation of each cell, and finally exits through the battery module outlet. Fig. 1(b) shows a sectional view of the module, where the batteries are arranged in a staggered pattern within the module. The air distribution pipes are located in the gaps of the staggered battery arrangement. The structural parameters of the air distribution pipes are shown in fig. 1(c). The pipes have a single inlet and dual outlets on the sides, and the bottom of the pipes is sealed to ensure that the cooling air flows out from the sidewalls of the pipes into the battery module.

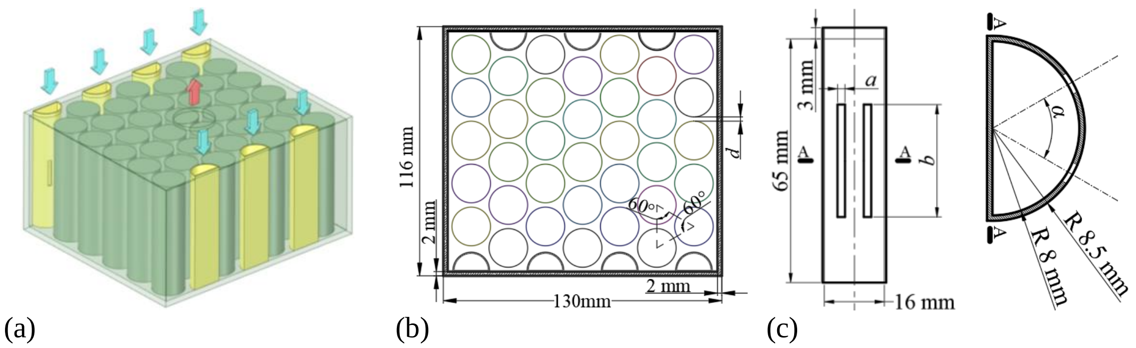

Figure 1. Air-cooled BTMS Structure and Its Components; (a) Battery Pack Model (b) Cross-sectional View of Battery Module in XY Plane (c) Air Distribution Pipe Structure

2.2. Numerical Model

In this paper, CFD is employed to simulate the fluid flow within the battery module and the heat exchange between the components and the fluid.

To determine the appropriate viscosity model, the Reynolds number (Re) is first calculated:

$$Re = \frac{\rho_a V \cdot d_h}{\mu} \tag{1}$$

Where ρ_a represents the coolant density, V stands for the average flow velocity of the fluid within the air-cooling pipe, d_h is the hydraulic diameter of the cooling channel, and μ is the dynamic viscosity coefficient of the fluid.

The maximum wind speed within the battery module is observed at the module outlet and the flow channel outlet, with the outlet dimensions of the air-cooling channel ranging is 30-225 mm^2. Air is used as the coolant, and at room temperature, the dynamic viscosity coefficient of air is denoted as 18.5×10^{-6} Pa×s The Reynolds numbers for several battery channel configurations have been calculated, with their values ranging is 4237-16023. Since the Reynolds number exceeds 4000, this study employs the turbulence model to simulate the turbulent flow within the battery module.

For the airflow within the model, the governing equations are as follows [23]:

Continuity equation:

$$\frac{\partial u}{\partial x} + \frac{\partial v}{\partial y} = 0 \tag{2}$$

Momentum equation:

$$\rho_b\left(u\frac{\partial u}{\partial x} + v\frac{\partial u}{\partial y}\right) = -\frac{\partial p}{\partial x} + \mu_1\left(\frac{\partial^2 u}{\partial x^2} + \frac{\partial^2 u}{\partial y^2}\right) \tag{3}$$

$$\rho_b\left(u\frac{\partial v}{\partial x} + v\frac{\partial v}{\partial y}\right) = -\frac{\partial p}{\partial y} + \mu_1\left(\frac{\partial^2 v}{\partial x^2} + \frac{\partial^2 v}{\partial y^2}\right) \tag{4}$$

Energy equation:

$$\rho c_p\left(u\frac{\partial T}{\partial x} + v\frac{\partial T}{\partial y}\right) = k\left(\frac{\partial^2 T}{\partial x^2} + \frac{\partial^2 T}{\partial y^2}\right) \tag{5}$$

Where u and v denote the Reynolds average velocity components, p is the Reynolds average pressure, ρ is the air density, μ_1 is the aerodynamic viscosity, c_p is the specific heat capacity of air, T represents the air temperature, and k is the air thermal conductivity.

Secondly, a thermal generation model for the battery cell is established based on the simplified theory proposed by Bernardi *et al*. in 1894 [24]:

$$Q = \frac{I}{V_b}\left[\left(E_0 - U_1\right) - T_1\left(\frac{dE_0}{dT_1}\right)\right] \tag{6}$$

Where Q represents the heat generation of the battery, V_b represents the volume of the battery, I represents the current, E_0 represents the open-circuit voltage, U_1 represents the working voltage, T_1 represents the system temperature, and (dE_0/dT_1) represents the temperature influence coefficient.

Finally, to provide a quantitative evaluation index for the designed BTMS, this paper introduces T_{max} as the maximum temperature of the battery module, T_{min} as the minimum temperature, and ΔT as the maximum temperature difference of the battery.

2.3. Boundary conditions

Each battery cell in the model has a capacity of 2.6 Ah, and the heat generation power of a single cell is determined through experiments and theoretical formulas, set as a volumetric heat source in this paper. The inlet is set as a velocity inlet, the outlet as a pressure outlet, and the fluid-solid coupling wall as a no-slip wall. The battery module casing exchanges heat with the environment through natural convection, with a heat transfer coefficient set to 5 W/m^{2}K. The contact surfaces between the battery, air distribution pipe, module casing, and cooling air are designated as fluid-solid coupling heat transfer surfaces. Finally, the ambient temperature is set to 26.5 °C, and the inlet air temperature is set to 25 °C. Detailed analysis parameters of numerical simulation are listed in tab. 1.

Table1. Detailed analysis parameters of numerical simulation

Component(s)	Housing (Aluminum)	Air pipe (Copper)	Battery	Coolant (Air)
ρ [kgm^{-3}]	2719	8978	2741	1.225
C [Jkg^{-1}k^{-1}]	871	381	1104	1106.4
K [Wm^{-1}k^{-1}]	202.4	387.6	1.6（Radial） 28（Axial）	0.0242

2.4. Grid independence test and Model Validation

To enhance the efficiency of CFD simulations and ensure the accuracy of the calculation results, it is essential to conduct a grid independence test and model validation before proceeding with the simulations.

Firstly, a mesh independence test is performed. The mesh employed is a polyhedral mesh with two boundary layers. Fig. 2(a) shows the meshing of the model and the meshing of the cross-section. The variation of the maximum temperature and temperature difference within the battery module concerning the number of mesh elements is illustrated in fig. 2(c). From the figure, it can be inferred that when the number of mesh elements exceeds 1,747,228, the impact of mesh quantity on temperature becomes negligible. However, further refining the mesh and improving its quality would significantly increase computational cost and time. Taking these factors into account, the number of mesh elements is controlled at around 1,747,228 in this study to facilitate subsequent calculations. At this mesh resolution, the minimum mesh quality is 0.3, and the maximum mesh quality is 0.837.

Secondly, the simulation model is verified. Fig. 2(b) is a schematic diagram of the experimental setup, where the entire experiment is conducted within a thermostat. A thermocouple is attached to the surface of a single battery, and the battery is charged/discharged through a charge/discharge tester, with the temperature data simultaneously recorded by a data collector. As shown in fig. 2(d), a comparison was made between the heat generation of the battery in the experiment with that in the model. At the end of charging and discharging, the maximum error between the experimental and simulated maximum temperatures is 0.72℃, which is still within the controllable range. Therefore, the simulation model is deemed reliable.

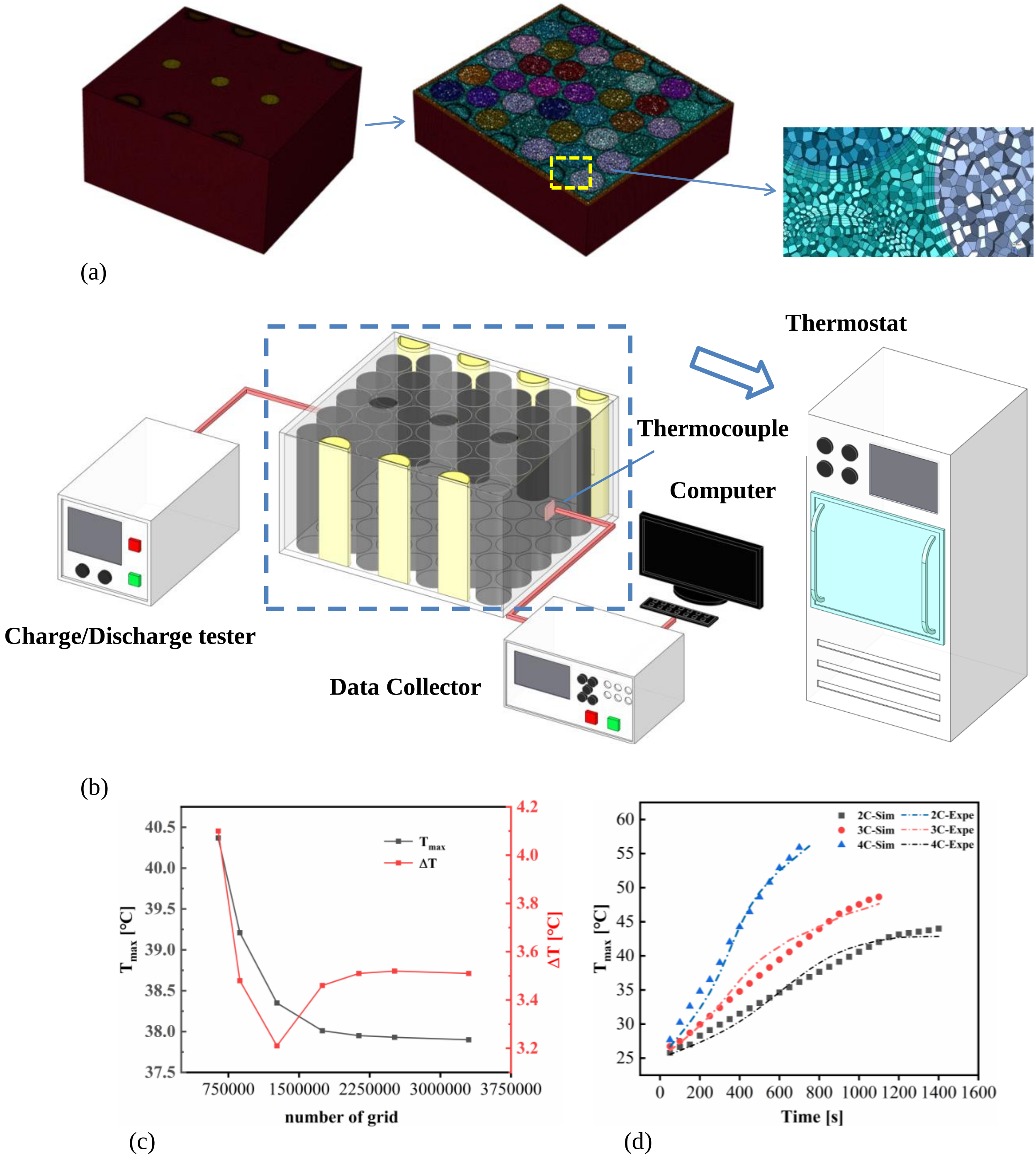

Figure 2. Grid and Model Validation; (a) Module Meshing (b) Schematic of experiment test platform (c) Verification of Mesh Independence (d) Thermal Model Validation

3. Comparison of Simulation Results

The study compares the performance of battery modules under three different structures: single inlet/outlet, double-layer reciprocating inlet/outlet, and structure with air distribution pipes. The inlet/outlet areas of the three models were kept consistent to ensure that the intake of cooling air into each module was the same at the same inlet velocity. Figs. 3(a-c) illustrates the model diagrams of these three structures and the temperature distribution of each battery module at a 2C charge/discharge rate under the same inlet velocity. Furthermore, during the simulation process, when applying the 2C charge/discharge condition to the battery, only the heat generation during the 2C charge/discharge process was considered. The heat generation curve obtained aligns with the one presented in Fig. 2(d).

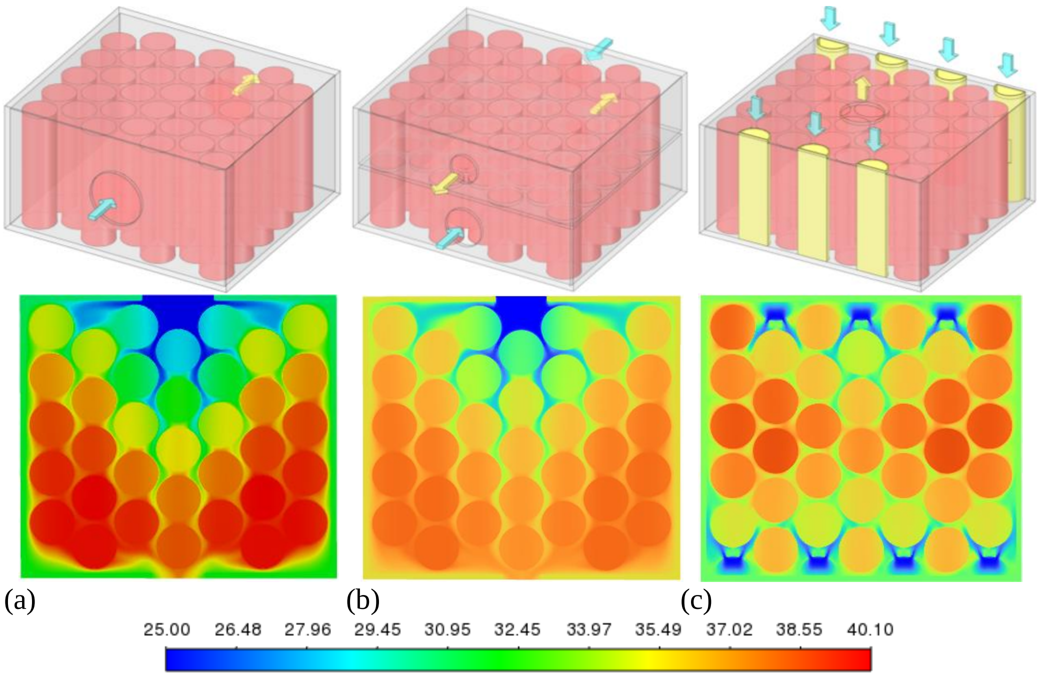

Figure 3. Temperature Contour Plots of Three Modules under Identical Conditions; (a) single inlet/outlet (b) double-layer reciprocating inlet/outlet (c) structure with air distribution pipes

Simulation results indicate that the air distribution pipe effectively alleviates the issue of temperature unevenness in traditional battery pack structures. The maximum temperature in fig. 3(a) appears at the edge of the module away from the inlet and outlet, reaching 40.28 °C, with a maximum temperature difference of 10.84 °C. The maximum temperature in fig. 3(b) appears in the middle two sides of the battery module, reaching 38.63 °C, with a maximum temperature difference of 5.32 °C. This reflects the insufficient heat dissipation capacity of structures (a) and (b) at locations far from the inlet and outlet. Fig. 3(c) shows that the temperature uniformity of the entire battery module is relatively consistent, with a maximum temperature difference of 4.78°C across the module. The highest temperature is concentrated in the middle area of the battery pack. This is because the air distribution ducts enable the cooling air to maintain a higher airspeed and sufficient cooling temperature when entering various parts of the module, while the staggered arrangement allows the cooling air to be more evenly distributed in every corner of the module. Under the combined effect of these two factors, the staggered arrangement with air distribution ducts can achieve better temperature performance than the traditional structure. Overall, the battery module with air distribution pipes is a feasible structure, can better leverage the natural advantages of the staggered arrangement, and effectively address the issue of maximum temperature difference.

4. Optimize the Air Distribution Device and Battery Module

4.1. The impact of spacing between batteries on the module

Next, a detailed analysis of each component of the battery module will be conducted to further optimize its performance. Firstly, the impact of the spacing between batteries will be investigated. This spacing not only influences the temperature distribution within the battery module but also has a direct effect on the energy density of the battery module. To assess this comprehensively, in addition to introducing the above-mentioned evaluation indices T_{max} and ΔT, S will also added as an evaluation metric for space utilization.

$$S = \frac{\text{volume of battery}}{\text{volume of module}} \tag{7}$$

Figs. 4(a) and 4(b) reflect the relationship between the spacing between batteries and the evaluation indicators T_{max}, ΔT, and S. The results indicate that when other parameters remain unchanged, the spacing between batteries has a significant impact on the maximum temperature difference within the battery module. When the spacing is increased from 1 mm to 1.5 mm and from 1.5 mm to 2 mm, the temperature difference changes by 0.67 °C and 0.72 °C. At the same time, as the spacing decreases, the maximum temperature also rises. Under the same changes, the maximum temperature increases by 0.61 °C and 0.58 °C, with a noticeable change in magnitude. This is because the reduced spacing will cause more cooling air to stagnate near the air inlet, and generate more turbulence at the small spacing, disrupting the normal airflow channel. This further reduces the amount of cooling air allocated to batteries that are farther away from the air inlet, which is unfavorable for the overall heat dissipation of the module. However, when the spacing is further increased from 2 mm, the airflow path becomes relatively fixed, and the impact of spacing on the overall temperature distribution of the module gradually weakens. Where the airflow paths remain stable when the module spacing is 2 mm and 3 mm. Considering space utilization and the temperature performance of the battery module, setting the spacing to 2 mm may be more suitable for this module. However, if further reduction of temperature difference and control of maximum temperature are required, the spacing can be increased.

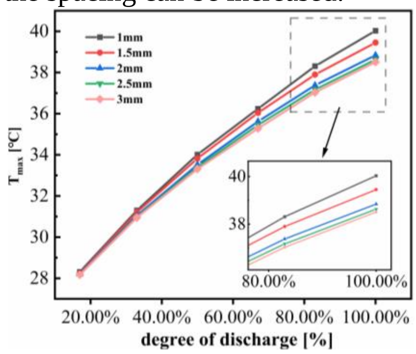

(a)

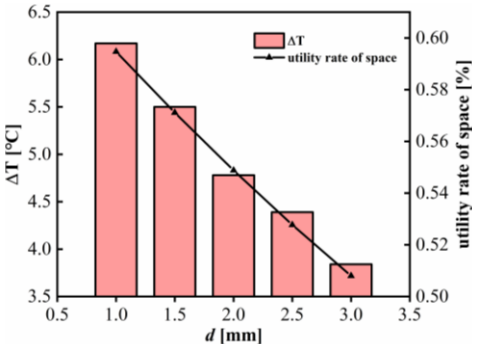

(b)

Figure 4. Influence of Battery Spacing on Various Evaluation Indicators; (a) effect of inter-battery spacing on maximum temperature (b) Effect of Inter-battery Spacing on Temperature Difference and Space Utilization Rate

4.2. The impact of changes in the module outlet on the battery module

When the battery arrangement remains unchanged, changes in the position of the battery module outlet will significantly impact the flow path of cooling air within the module. The primary goal of this section is to select an appropriate position for the battery module outlet to achieve optimal heat dissipation. The effects of changes in the position of the battery module outlet on the maximum temperature and maximum temperature difference of the battery module have been investigated at 2C charge/discharge when the inlet velocity is set to 2 m/s. Fig. 5 presents the velocity path line diagrams of the module under four different outlet configurations. In Case 1 and Case 2, the air outlets are located on both sides, while in Case 3 and Case 4, the air outlets are positioned at the top of the module. A comparative experiment is conducted when the air inlet velocity remains constant and the outlet area is controlled to be consistent. Observing the portions encircled in red in Fig. 5, it becomes evident that there are notable differences in airflow distribution at the top of the model across the four cases. Since the air pipes in this study are distributed along the sides of the model, the cooling effectiveness in the central region gradually diminishes due to reduced air velocity and increased temperature of the cooling air as it reaches the middle, resulting in the highest temperature occurring at the top center of the battery module. Having the outlets uniformly distributed on top allows the cooling air to converge, providing concentrated heat dissipation at the hottest points, which is highly beneficial for reducing the maximum temperature within the battery module. Therefore, Among the four different inlet and outlet configurations, the best temperature performance of the battery is observed in Case 4. In contrast, when the outlets are positioned on both sides (as in Cases 1 and 2), the airflow at the top center of the module is significantly reduced, and the outlets being closer to the pipe results in premature outflows of cooling air, causing a notable increase in temperature.

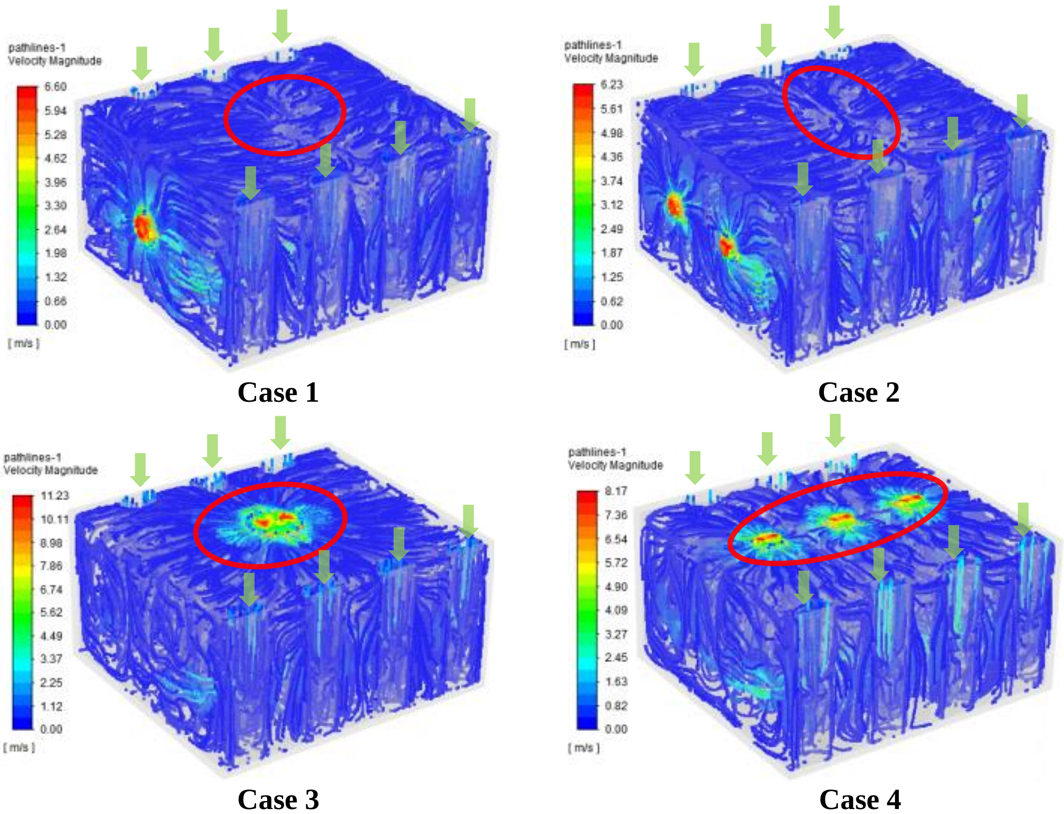

Figure 5. Velocity Trace Lines of Modules with Four Different Outlets

As shown in fig. 6, the temperature performance of the four cases can be observed. The maximum temperatures for Case 1 and Case 2 are 40.36 °C and 40.2 °C, respectively, with maximum temperature differences of 5.4 °C and 5.47 °C. However, for Case 3, the maximum temperature is reduced to 38.84 °C with a maximum temperature difference of 4.78 °C, indicating a significant improvement in overall temperature performance. Furthermore, Case 4 exhibits an even lower maximum temperature of 38.01 °C and a reduced maximum temperature difference of 3.46 °C. This demonstrates that adjusting the position of the module outlet has a notable impact on reducing battery temperatures.

This paper further discusses the size of the outlet based on Case 4. Enlarging the outlet can enhance heat exchange between the battery and the environment while reducing the outlet size facilitates the concentration of cooling air at the outlet. As shown in fig. 7, the battery exhibits the best overall temperature performance when the outlet radius is 6.5 mm.

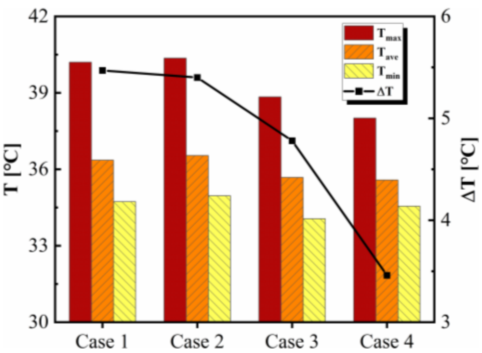

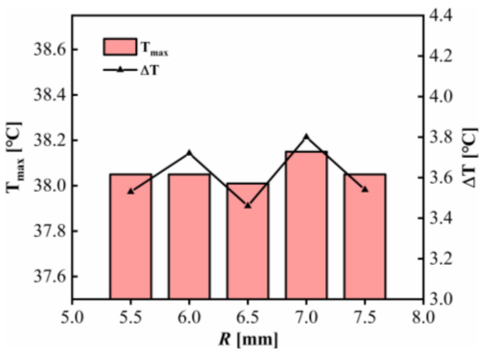

Figure 6. Temperature Performance of Each Case; Figure 7. Effect of Module Outlet Size on Maximum Temperature and Temperature Difference

4.3. The influence of air distribution pipe parameters on battery module performance

The structural parameters of the air distribution pipe directly affect the distribution of cooling air, which significantly influences the temperature distribution within the battery module. Therefore, this section focuses on optimizing the structural parameters of the air distribution pipes. The impact of air distribution pipe parameters on the maximum temperature and maximum temperature difference of the battery module under the conditions of an inlet velocity of 2 m/s and a battery charge/discharge rate of 2C was investigated.

Based on controlling the angle between adjacent outlets of the air pipe and the length of the air distribution pipe to remain unchanged, the width of the pipe outlet is controlled within the range of 1 mm to 5 mm. Fig. 8(a) shows the results of the maximum temperature and temperature difference varying with the width. It can be observed that the temperature performance of the battery pack deteriorates continuously as the outlet width is continuously increased from 1 mm to 5 mm. Similarly, Fig. 8(b) displays the results of the maximum temperature and temperature difference varying with the length. Similar conclusions can be drawn. This is because continuously enlarging the outlet size will lead to a reduction in the flow velocity of the cooling air, and the airflow will become less organized. As the cooling air passes through the highest temperature region in the module, its heat transfer capacity decreases due to the reduced flow velocity and unclear flow path.

Finally, the specific numerical values of each model in the single-factor analysis are presented, with the various parameters listed in the tab. 2.

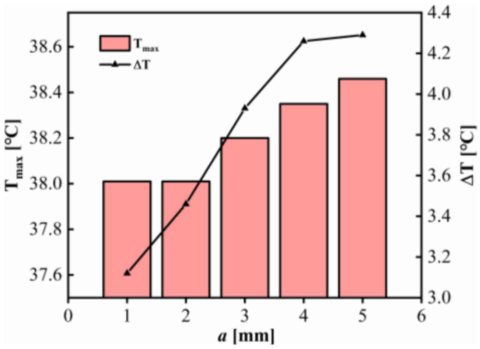

(a)

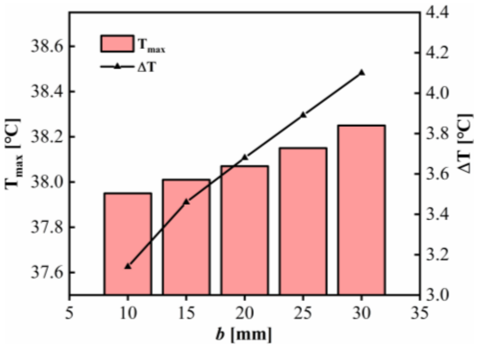

(b)

Figure 8. Influence of Air Pipe Outlet Parameters on Temperature; (a) Effect of Air Pipe Outlet Width on Temperature, (b) Effect of Air Pipe Outlet Length on Temperature

Table 2. Concrete Numerical Values of the Single-Factor Analysis Model

	Variables					
	a [mm]	*b* [mm]	*α* [°]	*d* [mm]	*Intake velocity*	*Charge/discharge rate*
Section 4.1	2	15	50	1 - 3	2 $m^{-1}s$	2C
Section 4.2	2	15	50	2	2 $m^{-1}s$	2C
Section 4.3 part 1	1 - 5	15	50	2	2 $m^{-1}s$	2C
Section 4.3 part 2	2	10 - 30	50	2	2 $m^{-1}s$	2C

4.4. Orthogonal experimental scheme and analysis

The various structures of the battery module do not independently affect the heat dissipation effect but rather influence the overall heat dissipation capability under the combined action of various factors. Therefore, it is necessary to comprehensively consider these factors to find a reasonable combination of parameters.

In the previous chapters, the single-factor analysis method was used to analyze various structural parameters of the battery module, but single-factor analysis alone cannot identify the optimal combination of parameters. Therefore, orthogonal experiments are needed to assist in this process. Finally, the results of the orthogonal experiment are subjected to both range analysis and variance analysis to evaluate the influence of each factor on the experimental results. The range refers to the difference between the maximum and minimum values of the experimental indicators under each level of a certain factor. Through range analysis, the degree of influence of each factor on the experimental results can be intuitively shown. In variance analysis, The P-value is used to evaluate the significance of the statistical test results, and this P-value is derived from the F-statistic. The formulas for calculating the range and the F-statistic are as follows:

$$R = X_{\max} - X_{\min} \tag{8}$$

$$F = \frac{SSB / dfB}{SSW / dfW} \tag{9}$$

Where X_{max} and X_{min} represent respectively the maximum and minimum values achieved by the experimental index under various levels of a certain factor. *SSB* is the Sum of Squares Between Groups, *SSW* is the Sum of Squares Within Groups, *dfB* is the Degrees of Freedom Between Groups, and *dfW* is the Degrees of Freedom Within Groups.

Based on the orthogonal experimental design, 25 experimental groups were established, and the simulation results are presented in the tab. 3. To determine the impacts of parameters a, b, α, and d on the battery module's T_{max} and ΔT, range and variance analyses were conducted on the outcomes of these orthogonal experiments. The results of these analyses are presented in the tab. 4.

Based on the range analysis, it is determined that when the outlet width of the distribution pipe (a) is 1 mm, the outlet length (b) is 10 mm, the angle between the outlets of the distribution air pipe s (α) is 40°, and the spacing between batteries (d) is 2 mm, the battery module experiences the lowest maximum temperature. Moreover, the temperature distribution of the battery module is most uniform when the outlet width (a) is 1 mm, the outlet length (b) is 10 mm, the angle between the outlets of the distribution air pipe s (α) is 60°, and the spacing between batteries (d) is 3 mm. Variance analysis reveals that the spacing between batteries (d) has a significant impact ($P<0.05$) on the maximum temperature difference within the battery module, while the other three factors have relatively minor effects. If a more uniform temperature distribution is prioritized, the spacing can be set to 3 mm. However, if greater emphasis is placed on the energy density and maximum temperature of the battery module, it is recommended to set the spacing to 2 mm.

4.5. Temperature performance of battery modules at various charge/discharge rates

Through orthogonal experiment analysis on the module, The optimal parameters for its structure are obtained. Finally, the batteries under different charge/discharge rates are placed in the optimized module for specific analysis, so as to obtain the optimal velocity of the module under each charge/discharge rate.

Fig. 9(a-c) shows the temperature curves at 2C, 3C, and 4C charge/discharge rates, respectively, under different inlet air velocities. It can be observed that at a 2C charge/discharge rate, an inlet air velocity of 2 m/s already satisfies the heat dissipation requirements (with a maximum temperature below 40 °C and a temperature difference within 5 °C). However, at a 3C charge/discharge rate, an inlet air velocity of 3 m/s is required. For a 4C charge/discharge rate, the battery requires an inlet air velocity of 5 m/s to meet the demand. It can be seen that as the charge/discharge rate increases, the required inlet air velocity rapidly escalates.

Table 3. Orthogonal Experimental Results

Model	a [mm]	b [mm]	α [°]	d [mm]	E	T_{max} [℃]	ΔT [℃]
1	1	10	40	1	1	37.81	3.38
2	1	15	60	2.5	5	38.59	3.4
3	1	20	80	1.5	4	38.25	4.24
4	1	25	50	3	3	38.48	3.73
5	1	30	70	2	2	38.05	3.49
6	2	10	80	2.5	3	38.51	3.92
7	2	15	50	1.5	2	38.11	3.92
8	2	20	70	3	1	38.44	3.29
9	2	25	40	2	5	38.18	4.09
10	2	30	60	1	4	38.84	5.13
11	3	10	70	1.5	5	38.26	3.68
12	3	15	40	3	4	38.44	4.18
13	3	20	60	2	3	38.27	3.96
14	3	25	80	1	2	38.97	5.26
15	3	30	50	2.5	1	38.54	4.15
16	4	10	60	3	2	38.64	3.91
17	4	15	80	2	1	38.38	4.03
18	4	20	50	1	5	38.9	5.2
19	4	25	70	2.5	4	38.5	3.82
20	4	30	40	1.5	3	38.71	4.91
21	5	10	50	2	4	38.39	4.33
22	5	15	70	1	3	38.9	5.01
23	5	20	40	2.5	2	38.5	4.3
24	5	25	60	1.5	1	38.73	4.77
25	5	30	80	3	5	38.54	3.98

Table 4. Range and Variance Analysis Results

Index	Importance of factors	Best solution		Range Value	Significance	
		Factors	Level		Factors	P
T_{max} [℃]	$d>a>\alpha>b$	a	1	0.39	a	0.17
		b	1	0.25	b	0.581
		α	1	0.29	α	0.483
		d	3	0.43	d	0.176

ΔT [℃]	$d>a>b>\alpha$	a	1	0.83	a	0.087
		b	1	0.49	b	0.396
		α	3	0.43	α	0.518
		d	5	0.98	d	0.034

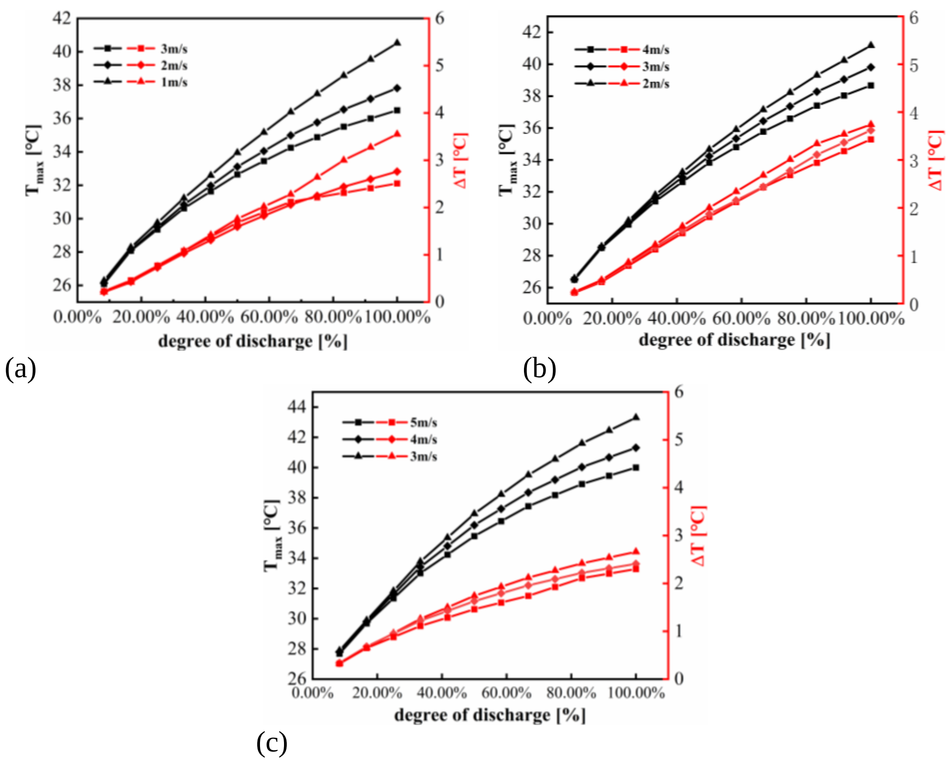

Figure 9. (a-c) Temperature Curves for Charging/Discharging Rates of 2C, 3C, and 4C at Different Inlet Air Velocities

5. Conclusion

In this paper, addressing the issues of traditional staggered arrangements, such as high-temperature rise, large temperature differences, and the additional volume and complexity of incorporating air pipes, a novel staggered arrangement with an air distribution pipe is proposed, and this structure is analyzed and studied in detail. The battery module consists of 35 individual cells, with the air pipe placed in the gaps of the staggered arrangement to uniformly distribute air and improve the temperature uniformity of the battery module while reducing the maximum temperature. The CFD method is used to analyze the battery module structure and air pipe configuration. The conclusions are summarized as follows:

1. Compared with the traditional staggered arrangement structure, both T_{max} and ΔT of the staggered arrangement structure with air distribution pipe have a certain degree of decline, with T_{max} decreasing by 2.47 °C, and the decline in ΔT is particularly pronounced, reaching 74.5%.

2. The optimal structural parameters for the BTMS are a model outlet radius of 6.5 mm, outlet width of the distribution pipe (a) = 1 mm, outlet length (b) = 10 mm, the spacing between batteries (d) = 2mm, the angle between the outlets of the distribution air pipes (α) = 40°, Compared to the initial model, the improved optimal model achieves a reduction of 1.03 °C in the maximum temperature and a 42.26% decrease in the temperature difference.

3. To meet the heat dissipation requirements at 2C, 3C, and 4C charge/discharge rates, the required inlet air velocities are 2 m/s, 3 m/s, and 5 m/s, respectively. As the charge/discharge rate increases, the required inlet air velocity also rapidly increases.

References

[1] M.A. Hannan., *et al*., A Review of Lithium-Ion Battery State of Charge Estimation and Management System in Electric Vehicle Applications: Challenges and Recommendations, *Renewable and Sustainable Energy Reviews, 78* (2017), 1, pp. 834-854.

[2] H. Ge., *et al*., Temperature-Adaptive Alternating Current Preheating of Lithium-Ion Batteries with Lithium Deposition Prevention, *Journal of The Electrochemical Society, 163* (2015), 1,pp. 290-299.

[3] Y. Ding., *et al*., A Short Review on Layered $LiNi_{0.8}Co_{0.1}Mn_{0.1}O_2$ Positive Electrode Material for Lithium-Ion Batteries, *Energy Procedia, 105* (2017), 1,pp. 2941-2952.

[4] H.J. Noh., *et al*., Comparison of the Structural and Electrochemical Properties of Layered Li $[Ni_xCo_yMn_z]$ O_2 (x= 1/3, 0.5, 0.6, 0.7, 0.8 and 0.85) Cathode Material for Lithium-Ion Batteries, *Journal of Power Sources 233* (2013), 2,pp. 121-130.

[5] F.L. Yun., *et al*., Thermal Behavior Analysis of a Pouch Type Li $[Ni_{0.7}Co_{0.15}Mn_{0.15}]$ O_2-Based Lithium-Ion Battery, *Rare Metals, 35* (2016), 2,pp. 309-319.

[6] Ouyang., *et al*., Impact of High-Temperature Environment on the Optimal Cycle Rate of Lithium-Ion Battery, *Journal of Energy Storage 28* (2020), 1,pp. 101242.

[7] Ouyang., *et al*., Electrochemical and Thermal Characteristics of Aging Lithium-ion Cells after Long-Term Cycling at Abusive-Temperature Environments, *Process Safety and Environmental Protection 159* (2022)), 1,pp. 1215-1223

[8] Jaguemont., *et al*., A Comprehensive Review of Lithium-Ion Batteries Used in Hybrid and Electric Vehicles at Cold Temperatures, *Applied Energy 164* (2016), 1,pp. 99-114.

[9] T. Dong, *et al*., Numerical Modeling and Analysis of the Thermal Behavior of NCM Lithium-Ion Batteries Subjected to Very High C-rate Discharge/Charge Operations, *International Journal of Heat and Mass Transfer 117* (2018), 1,pp. 261-272.

[10] M. Malik, *et al*., Thermal and Electrical Performance Evaluations of Series Connected Li-Ion Batteries in a Pack with Liquid Cooling, *Applied Thermal Engineering 129* (2018), 10,pp. 472-481.

[11] X.P. Du, *et al*., Experimental Investigation on Mini- Channel Cooling–Based Thermal Management for Li- Ion Battery Module Under Different Cooling Schemes, *International Journal of Energy Research 42* (2018), 2,pp. 2781-2788.

[12] R. Mahamud, C. Park., Reciprocating Air Flow for Li-Ion Battery Thermal Management to Improve Temperature Uniformity, *Journal of Power Sources 196* (2011), 2,pp. 5685-5696.

[13] S. Park, D.H. Jung., Battery Cell Arrangement and Heat Transfer Fluid Effects on the Parasitic Power Consumption and the Cell Temperature Distribution in a Hybrid Electric Vehicle, *Journal of Power Sources 227* (2013), 2,pp. 191-198.

[14] A. Jarrett, I.Y. Kim., Influence of Operating Conditions on the Optimum Design of Electric Vehicle Battery Cooling Plates, *Journal of Power Sources 245* (2014), 2,pp. 644-655.

[15] Z.Y. Ling, *et al*., A Hybrid Thermal Management System for Lithium-Ion Batteries Combining Phase Change Materials with Forced-Air Cooling, *Applied Energy 148* (2015), 2,pp. 403-409.

[16] Wu, Mao-Sung, *et al*., Heat Dissipation Design for Lithium-Ion Batteries. *Journal of Power Sources 109* (2002), 1,pp. 160-166.

[17] N. Yang, *et al*., Assessment of the Forced Air-Cooling Performance for Cylindrical Lithium-Ion Battery Packs: A Comparative Analysis Between Aligned and Staggered Cell Arrangements, *Applied Thermal Engineering 80* (2015), 10,pp. 55-65.

[18] T. Wang, *et al*., Thermal Investigation of Lithium-Ion Battery Module with Different Cell Arrangement Structures and Forced Air-Cooling Strategies, *Applied Energy 134* (2014), 9,pp. 229-238.

[19] Lu, *et al*., Parametric Study of Forced Air Cooling Strategy for Lithium-Ion Battery Pack with Staggered Arrangement, *Applied Thermal Engineering 136* (2018), 12,pp. 28-40.

[20] Yang, *et al*., Optimization Study of Air-Cooled Stagger-Arranged Battery Pack with Reverse-Layered Airflow, *Journal of Energy Storage 55* (2022), 11,pp. 105524.

[21] Zhou, *et al*., Thermal Performance of Cylindrical Lithium-Ion Battery Thermal Management System Based on Air Distribution Pipe. I*nternational Journal of Heat and Mass Transfer 131* (2019), 3,pp. 984-998.

[22] Yang, *et al*., Thermal Performance of Honeycomb-Type Cylindrical Lithium-ion Battery Pack with Air Distribution Plate and Bionic Heat Sinks. *Applied Thermal Engineering 218* (2023), 3,pp. 119299.

[23] Luo, *et al*., Optimal Structure Design and Heat Transfer Characteristic Analysis of X-Type Air-Cooled Battery Thermal Management System. *Journal of Energy Storage 67* (2023), 3,pp. 107681.

[24] Bernardi, D., *et al*., A General Energy Balance for Battery Systems. *Journal of the Electrochemical Society 132* (1985), 1, pp. 5-12

Paper submitted: 03.08.2024

Paper revised: 17.09.2024

Paper accepted: 22.09.2024